Site Identification of Mixed Arrays of Keggin-type Heteropolyacids by Scanning Tunneling Microscopy and Tunneling Spectroscopy

Mahmoud S. Kaba, In K. Song,† and Mark A. Barteau*

Center for Catalytic Science and Technology, Department of Chemical Engineering, University of Delaware, Newark, Delaware 19716

Received: December 4, 2001

Scanning tunneling microscopy (STM) and tunneling spectroscopy (TS) studies on the mixed arrays of Keggin-type heteropolyacids (HPAs) deposited on a highly oriented pyrolytic graphite (HOPG) surface were carried out to test the ability of these techniques to distinguish structurally similar molecules. An equimolar aqueous mixture of HPAs was deposited on a graphite surface for STM measurements. The mixture of Keggin-type HPAs, $H_3PW_{12}O_{40}$ and $H_3PMo_{12}O_{40}$, with identical net anionic charges and identical charge-compensating cations (protons), formed ordered two-dimensional arrays on a graphite surface similar to those formed by their pure components. The periodicities of the arrays were in good agreement with the shape and dimension of the pure Keggin HPAs. It was evident from the STM image of the mixed array that some features appeared brighter than others; the ratio of bright to dim features was almost unity as designed, and their distribution within the ordered array on the surface appeared to be random. TS measurements revealed that the bright corrugations were $[PW_{12}O_{40}]^{3-}$ anions and that the less bright ones were $[PMo_{12}O_{40}]^{3-}$ anions. It is successfully demonstrated that HPAs with indistinguishable geometric structures and sizes can be distinguished based on differences in their electronic properties using STM operated in air.

Introduction

Although one of the main uses of scanning tunneling microscopy (STM) continues to be the elucidation of surface structures,[1−3] the ability of this technique to resolve both position and chemical identity on an atomic level in real space makes it well-suited for studying chemical processes on surfaces. Much interest has been focused on the chemical identity, bonding geometry, adsorption sites, and packing of chemisorbed species.[4−7] In principle, the orientation of molecules with respect to the underlying surface plane should be observable by STM, as well as the structure of chemisorbed species including reactants, products, and some reactive intermediates. Such information could, in turn, help elucidate reaction mechanisms and perhaps lead to the design of novel surfaces, especially of solid catalysts, in order to carry out reactions selectively.

An important step toward real space imaging of chemical reactions on surfaces, and thus to our understanding of chemical reaction pathways or mechanisms, is the ability to image mixtures of two different adsorbed species and to distinguish between them by scanning tunneling microscopy (STM). The task is a little easier when there are significant differences between the sizes of the different species, but difficult when they are similar in structure and size. In principle, tunneling spectroscopy (TS) can be utilized, in conjunction with the STM image, to distinguish between chemically inequivalent adsorbates with essentially identical geometric structures and sizes. The distinction is made based on differences in electronic structures.

The ability to distinguish between closely related molecules is of great importance in applications where molecular recognition or sequencing is desired. Early ultra-high-vacuum (UHV) studies showed that the STM can distinguish between two different molecules (carbon monoxide and benzene)[8] and between two similar molecules (naphthalene and azulene)[9] coadsorbed onto metal surfaces. In both cases, the distinction was made based on the resolution of specific structural features associated with each molecule. The first study demonstrated the first definitive identification of two types of adsorbed molecules on a surface with high spatial resolution.[8] Such resolution was only attainable at very low voltages (applied potential between the STM tip and the sample surface) for which the tip was very close to the surface and contributions from the molecular states appeared near the Fermi level (E_F).[8] A further example of molecular discrimination was provided by Boland and Villarrubia, in which they showed that the products from the reaction of chlorine with the Si(111)−(7 × 7) surface could be identified by registries and by sizes using STM.[10] Also, Wouda et al.[11] reported that different metal atoms on a alloy surface could be identified by the apparent height difference of more than 20 pm in the STM image. Structurally identical but electronically inequivalent mixed arrays of metal phthalocyanines on Au(111) have been imaged by STM, and individual sites were distinguished by metal d-orbital occupation-dependent images.[12,13] More recently, organic species adsorbed on a metal surface, for example, *m*-xylene and *p*-xylene on Pd(111),[14] have been imaged and distinguished using STM. A more complicated system related to adsorption and chemical reaction, methoxy and formate species on Cu(110) surfaces resulting from reactions of methyl formate, methanol, and formic acid,[15] was also successfully probed by STM.

In general, it is difficult to resolve the molecular structures of adsorbates on surfaces. The difficulties may arise from rapid surface diffusion, electric field effects,[16] or the absence of molecular states near E_F. When one cannot easily distinguish

* To whom correspondence should be addressed. Telephone: (302) 831-8905. Fax: (302) 831-8201. E-mail: barteau@che.udel.edu..

† Present address: Department of Industrial Chemistry, Kangnung National University, Kangnung 210-702, Korea.

10.1021/jp014401s CCC: $22.00
Published on Web 02/07/2002

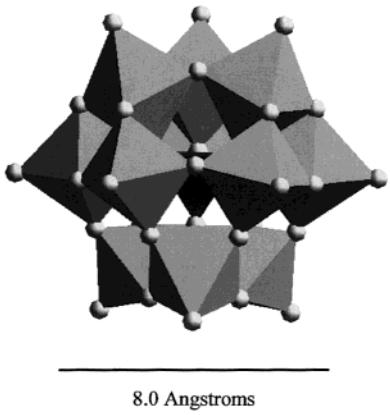

Figure 1. Polyhedral representations of the molecular structure of Keggin-type heteropolyanion $[PW_{12}O_{40}]^{3-}$.

between chemically inequivalent sites or adsorbates with nearly identical geometric structures and sizes, or when the STM image is of low resolution, one may resort to tunneling spectroscopy (TS). The STM image is a convolution of both the geometric and electronic structures of the surface, but TS probes only electronic states. Current−voltage ($I-V$) characteristics have been utilized, for example, to distinguish between reacted and unreacted dangling bond sites on adsorbate-covered Si surfaces.[17−20] In a STM study on the initial stages of Li adsorption on Si(001) surface, Johansson et al.[21] showed that two types of Li clusters formed on Si(001) surface could be discriminated by their $I-V$ spectra. Additionally, Bode et al.[22] grew thin films of Fe on W(110) and showed that the tunneling spectra of the Fe sites changed drastically when probed with a ferromagnetic iron-covered W tip as opposed to a clean W tip; no such changes were observed in the spectra of the W sites. The changes in the electronic properties of the former sites were presumably related to the magnetic properties of that system. That study[22] not only showed that chemically inequivalent sites could be distinguished by STM (or more specifically by TS), but it also exemplified the role of the tip in STM or TS. Hence, it is prudent to ensure that data are reproducible by using different tips and samples when making STM or TS measurements.

In this work, nanoscale site-by-site examination of mixed arrays of Keggin-type heteropolyacids (HPAs) was carried out by scanning tunneling microscopy and tunneling spectroscopy for site identification of individual molecules from mixed arrays. A mixture of Keggin-type[23] HPAs having both similar molecular size and identical anionic charge was used to form the arrays. The identity of individual HPAs was determined by their electronic properties. This is potentially an important step for the creation and characterization of complex reactive surface structures from molecular components.

Figure 1 shows the polyhedral representation of the molecular structure of a typical Keggin-type[23] heteropolyanion, $[PW_{12}O_{40}]^{3-}$, as determined from published X-ray diffraction (XRD) data.[24] The size of Keggin-type anions is ca. 10−12 Å, and the anion has a pseudospherical shape. The molecular structure of $[PW_{12}O_{40}]^{3-}$ consists of a heteroatom, P, at the center of the anion cluster, tetrahedrally coordinated to four oxygen atoms. This tetrahedron is surrounded by 12 WO_6 octahedra. HPAs are d^0 early transition metal oxygen anion clusters, and they are well-known as acid catalysts,[25,26] oxidation catalysts,[27,28] and electrode functionalization agents.[29]

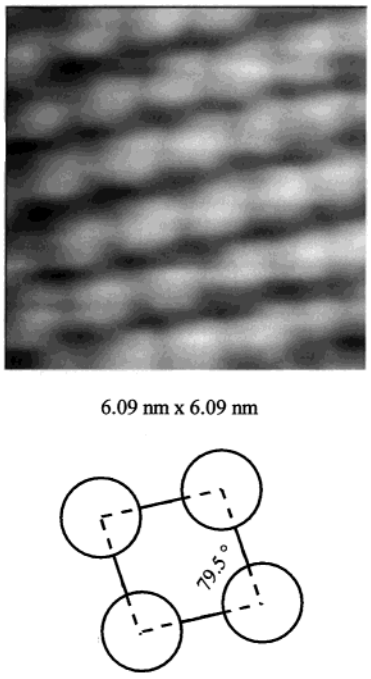

Figure 2. STM image of $H_3PW_{12}O_{40}$ deposited on graphite.

Experimental Section

Sample Preparation and Deposition. The Keggin-type[23] heteropolyacids, $H_3PW_{12}O_{40}$ and $H_3PMo_{12}O_{40}$, were obtained from Aldrich Chemical Co. (Milwaukee, WI). Approximately 0.01 M aqueous solutions of each sample were then prepared in order to make equimolar mixed solutions for the STM measurements. A drop of the single or mixed solution was deposited on a freshly cleaved highly oriented pyrolytic graphite (HOPG) surface and allowed to dry in air or in a desiccator in order to minimize bulk crystal formation.

STM and TS Measurements. STM images were acquired using a TopoMetrix TMX-2010 Discoverer instrument. Mechanically formed $Pt_{0.9}Ir_{0.1}$ tips were used. STM images were acquired in the constant current mode at a tunneling current of 1−2 nA and a sample bias of 100 mV. Calibration procedures have been described elsewhere.[30,31] No image presented in the present work was Fourier filtered. TS measurements were taken using both the TopoMetrix and the LK Technologies LK 1000 instruments to confirm consistency and reproducibility. TS measurements were performed at least 10 times each using at least three different tips for each sample to obtain more accurate and reproducible results, and to provide a basis for statistical analyses. The STM probe was positioned above the corrugation (heteropolyanion) of interest for the TS measurements, and the tunneling current was monitored while the bias voltage was ramped from −2 to +2 V. The voltage axis in the tunneling spectrum represents the potential applied to the sample relative to that of the tip.

Results and Discussion

Site Identification of $H_3PW_{12}O_{40}$ and $H_3PMo_{12}O_{40}$ by STM. Experiments were designed to examine the mixed arrays of Keggin-type HPAs with the same net charge and countercations, namely $H_3PW_{12}O_{40}$ and $H_3PMo_{12}O_{40}$, in order to minimize the potential influences of anion size, net charge, or countercation identity on the formation of well-ordered mixed arrays. Figures 2 and 3 show STM images of pure $H_3PW_{12}O_{40}$ and $H_3PMo_{12}O_{40}$ arrays on graphite surfaces, respectively. These images clearly indicate the formation of ordered and self-

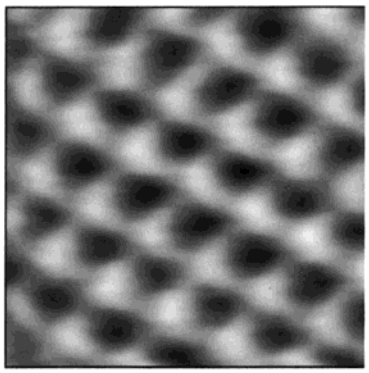

Figure 3. STM image of $H_3PMo_{12}O_{40}$ deposited on graphite.

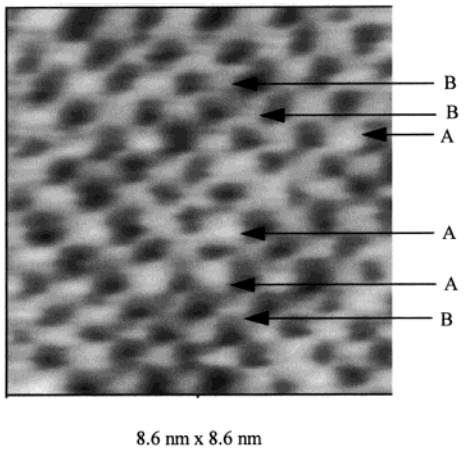

Figure 4. STM image of the mixed array of $H_3PW_{12}O_{40}$ and $H_3PMo_{12}O_{40}$ on HOPG.

assembled arrays on the graphite surface. The periodicity of the $H_3PW_{12}O_{40}$ array is 11.7 Å, and that of the $H_3PMo_{12}O_{40}$ array is 10.8 Å. The unit cells shown below each image were constructed on the basis of lattice constants determined from two-dimensional fast Fourier transforms (2D-FFT). These show that the arrays of $H_3PW_{12}O_{40}$ and $H_3PMo_{12}O_{40}$ have nearly square symmetry; the array symmetry of $H_3PW_{12}O_{40}$ and $H_3PMo_{12}O_{40}$ was similar, with included angles α of 79.5° and 84.9°, respectively. The periodicities and included angles of these HPA arrays varied little from scan to scan of either sample, and the reported lattice constants (which are consistent with previous results[30−35]) are average values determined from at least three images for each sample. HPA samples examined here formed well-ordered arrays on graphite surfaces over scan areas of at least 200 Å by 200 Å. As observed previously,[30,31] tunneling spectra obtained at the interstices (darkest features in Figures 2−4) were the same as those obtained from bare graphite surfaces, demonstrating that the HPA arrays in these images are monolayers.

Figure 4 shows the STM image of a mixed array of $H_3PW_{12}O_{40}$ and $H_3PMo_{12}O_{40}$ deposited from an equimolar

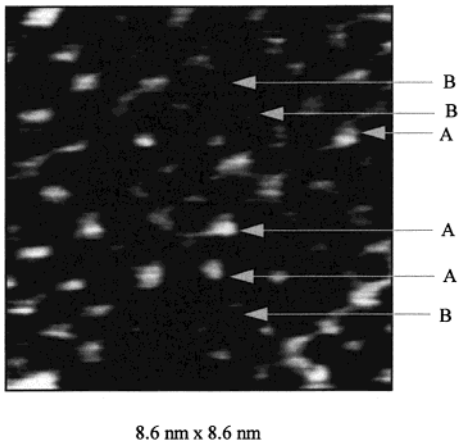

Figure 5. Contrast-enhanced image of Figure 4.

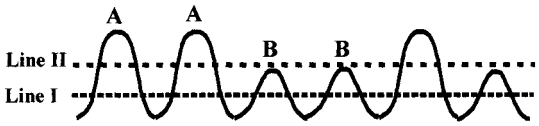

Figure 6. Line scan schematic depicting the STM contours of the mixed array in Figure 4 (initial, line I) and after the image contrast was enhanced as shown in Figure 5 (enhanced, line II).

mixture on graphite. From this high resolution image, one can clearly see a well-ordered two-dimensional array with a periodicity of 11.0 Å which is consistent with the dimensions of the Keggin anion determined by STM[26,28,30−35] and X-ray crystallography.[24] The array symmetry of the HPA mixture is also nearly rectangular (α= 80.4°). These results suggest that the array characteristics of the pure components appear to be maintained in the mixture. This may be a result of the equivalence of the size, net charge of the $[PW_{12}O_{40}]^{3-}$ and $[PMo_{12}O_{40}]^{3-}$ polyanions, and the identity and number of charge-compensating protons.

More importantly from Figure 4, one can observe corrugations whose contrast relative to the dark interstices falls mainly into two categories—those that are very bright (labeled A) and those that are less bright (labeled B). While this may not seem obvious to the not-so-well trained eye, one can use the image enhancement software of the STM to establish a threshold (or height minimum) for the image height or contrast, and thus accentuate the contrast of the higher contrast corrugations and mask those regions with heights less than the threshold. Such an enhanced image is shown in Figure 5. Also, a line scan schematic showing how the corrugations appear after the threshold is established is shown in Figure 6. If the threshold is set at the level designated I, the features labeled A and B in Figure 6 are imaged as very bright and less bright corrugations, respectively, as imaged in Figure 4. If the threshold is set at level II, however, corrugations labeled A in Figure 6 are the only features resolved, as shown in Figure 5. The enhanced image in Figure 5 clearly shows remaining bright spots (sites A) which represent almost half of the corrugations in the original image. The criterion for identifying a bright corrugation is one whose diameter is at least half its initial diameter (prior to the image enhancement). If one ascribes these bright corrugations to one kind of Keggin polyanion, then the surface coverage is consistent with its concentration in the mixture, which is equimolar, and the distribution of the anions in the mixed array is fairly random, as illustrated by the map shown in Figure 7, corresponding to the image in Figure 4.

Often in the interpretation of STM images image height is used interchangeably with image contrast; that is, the higher a

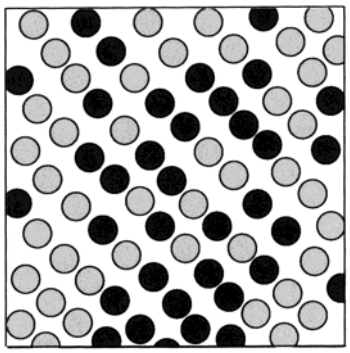

Figure 7. Schematic of the mixed array of $H_3PW_{12}O_{40}$ and $H_3PMo_{12}O_{40}$ on HOPG shown in the STM image of Figure 4. The darker circles represent $[PMo_{12}O_{40}]^{3-}$ anions, while the lighter circles represent $[PW_{12}O_{40}]^{3-}$ anions.

feature on the sample surface, the brighter that feature in the image. Considerable care is warranted, however. For example, an STM image of Xe atoms physisorbed on a Ni(110) surface showed the contours of Xe atoms having a height of 1.6 Å relative to the Ni surface.[36] This height was considerably less than that (2.7 Å) calculated from a hard sphere model, indicating that the STM contour was not simply a representation of the van der Waals surface of the adsorbates. In general, the image can be considered as a surface topograph when the features resolved are on the nanometer scale or larger, but this definition may not hold at the atomic scale since it is not clear as to what a topograph at this level really is.[37] The most reasonable definition of the topograph is that it represents contours of constant surface charge density. Thus, in contact-mode atomic force microscopy (AFM) measurements where all of the electrons of the surface atoms are involved in the repulsive interactions with the AFM tip, the AFM image can be reasonably described as a total electron density map of the surface.[38] However, this interpretation can be misleading, especially for the STM, because the only electrons that contribute to tunneling are those near E_F. Thus, neglecting tip−sample interactions, the STM image can be described by the partial electron density plot, $r(r_0,E_F)$, of the sample surface, or as contours of constant local density of states (LDOS). Adsorbates on metal surfaces usually modify the LDOS near E_F by electronic states derived from the adsorbate orbitals.[39] This "mixing" of orbitals and their proximity to the tip make it possible to image these adsorbates. STM images showing the atomic- and molecular-scale features of a large number of organic and inorganic layered materials[40] have been successfully interpretated on the basis of the $r(r_0,E_F)$ plots calculated using the extended Hückel tight binding (EHTB) electronic band structure method.[41] The contribution of an atom to the $r(r_0,E_F)$ generally increases as its distance from the tip decreases and as its electronic contribution to the energy levels near the Fermi level increases.[42] This does not imply that the more protruding atoms would make more contributions to the energy levels near E_F, and hence would appear bright in the image. Rather, the relative electronic contributions based on their electronic structures would determine their relative contrast in the STM image. Therefore, the difference in the contrast of the corrugations seen in the STM images of Figures 4 and 5 is a reflection of the different electronic contributions from each kind of polyanion in the mixture, reflecting their different electronic structures. A previous quantum chemical study[43] of the frontier molecular orbitals of HPAs has clearly delineated differences in electronic structure between $H_3PW_{12}O_{40}$ and $H_3PMo_{12}O_{40}$.

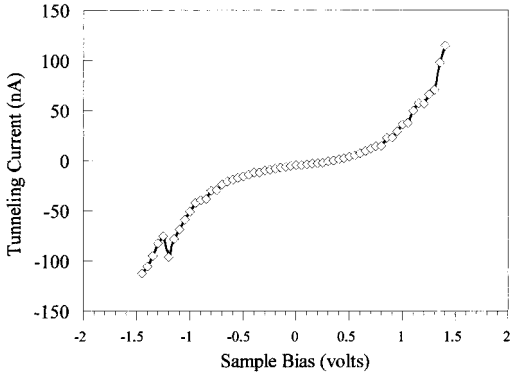

Figure 8. $I-V$ spectrum of an $H_3PW_{12}O_{40}$ monolayer.

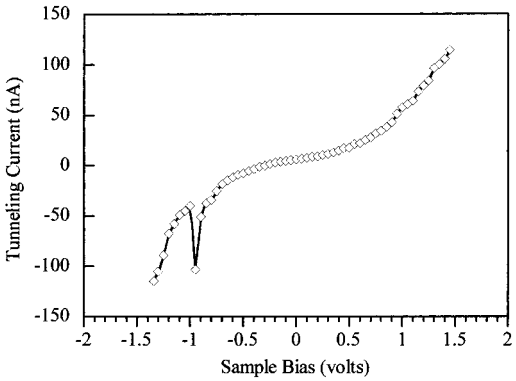

Figure 9. $I-V$ spectrum of an $H_3PMo_{12}O_{40}$ monolayer.

In HPAs, the HOMO (highest occupied molecular orbital) consists primarily of nonbonding p-orbitals on the oxygens of the HPAs, while the LUMO (lowest unoccupied molecular orbital) consists of an antibonding combination of d-orbitals on the metal centers and p-orbitals on the neighboring bridging oxygens. This implies that both HPA samples have almost the same HOMO energy, but different LUMO energy. The energy gaps between the LUMO and the HOMO were reported to be 2.0 eV for $H_3PW_{12}O_{40}$ and 1.7 eV for $H_3PMo_{12}O_{40}$.[43]

Site Identification of $H_3PW_{12}O_{40}$ and $H_3PMo_{12}O_{40}$ by Tunneling Spectroscopy. It has been observed that HPAs exhibit a distinctive current−voltage ($I-V$) behavior referred to as negative differential resistance (NDR) at specific applied voltages in their tunneling spectra.[31,33−35] STM images in this work were obtained at positive sample biases with respect to the tip. NDR behavior for HPA samples is observed at negative sample biases, i.e., when electrons tunnel from sample to tip. We have demonstrated that NDR peak position not only serves as a fingerprint of HPA identity,[34] but it also correlates well with the reduction potential (electronic property) of HPAs.[31,33,35] NDR behavior observed in electrically insulating materials has been explained in terms of resonant tunneling through a double barrier quantum well.[44−46] However, the detailed mechanism of NDR for the HPA samples has not yet been elucidated.

Figures 8 and 9 show typical $I-V$ curves of pure $H_3PW_{12}O_{40}$ and $H_3PMo_{12}O_{40}$ HPAs taken at corrugations in Figures 2 and 3, respectively. The NDR peak voltage was defined in this work as the voltage where the maximum current was observed in the distinctive $I-V$ region. The NDR peak voltages of $H_3PW_{12}O_{40}$ and $H_3PMo_{12}O_{40}$ in these two spectra were −1.20 and −0.95 V, respectively, near the statistical averages measured for these two molecules, as discussed below. Tunneling spectra taken at the interstitial spaces between bright corrugations in Figures 2 and 3 exhibited the typical $I-V$ response of graphite, indicating that the two-dimensional arrays of $H_3PW_{12}O_{40}$ and $H_3PMo_{12}O_{40}$

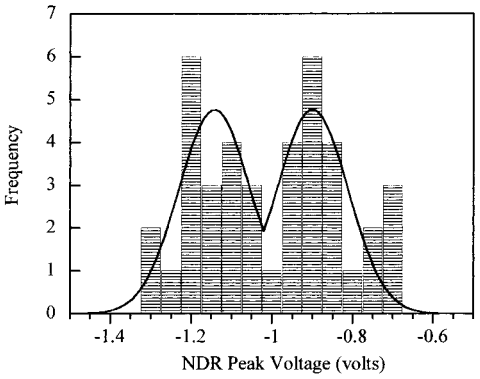

Figure 10. Frequency distribution of NDR peak voltages in the mixed array of $H_3PW_{12}O_{40}$ and $H_3PMo_{12}O_{40}$. The distribution is bimodal with statistical means of -1.15 ± 0.05 V and -0.90 ± 0.05 V.

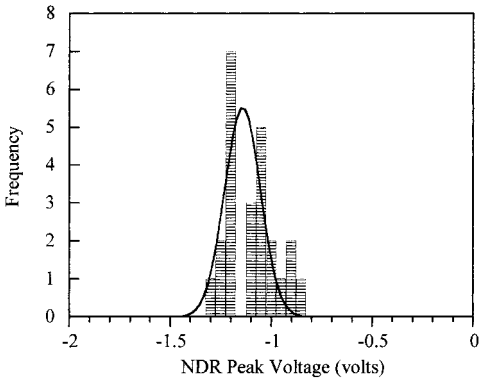

Figure 11. Frequency distribution of NDR peak voltages in the pure $H_3PW_{12}O_{40}$ monolayers. The distribution is monomodal with a statistical mean of -1.14 ± 0.09 V.

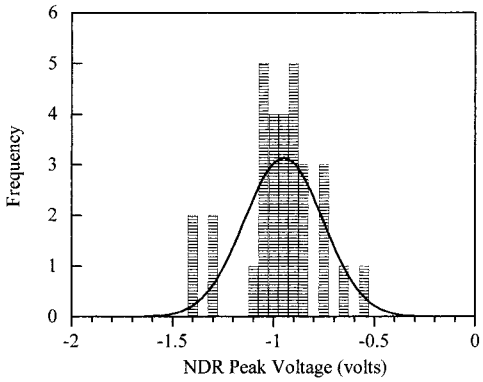

Figure 12. Frequency distribution of NDR peak voltages in the $H_3PMo_{12}O_{40}$ monolayers. The distribution is monomodal with a statistical mean of -0.95 ± 0.09 V.

are monolayers at least in this region imaged, as previously demonstrated.[31,33,34] An important criterion in spectroscopic studies of mixed arrays is that the difference between the NDR voltages of the pure components be significantly greater than the accuracy of the TS measurements, ca. 50 mV or less (depending on the instrument being used). This is important because the heteropolyanions $[PW_{12}O_{40}]^{3-}$ and $[PMo_{12}O_{40}]^{3-}$ have the same Keggin structure and almost the same molecular dimensions. Since the lateral resolution of the STM would not necessarily be expected to show the slight differences in the dimensions of the heteropolyanions under our imaging conditions, differentiation between different HPAs in the mixture must be based solely on their electronic properties.

Further evidence that the electronic structures of the corrugations ("bright" vs "dim" heteropolyanion features in Figures 4 and 5) differ can be garnered from spatially resolved tunneling spectroscopy measurements. The characteristic NDR peak voltages of a mixed array of $H_3PW_{12}O_{40}$ and $H_3PMo_{12}O_{40}$ were measured to identify the individual molecules by their electronic properties. Tunneling spectra taken at the interstitial spaces between corrugations in Figure 4 showed the typical $I-V$ response of graphite, also indicating that the two-dimensional mixed array of $H_3PW_{12}O_{40}$ and $H_3PMo_{12}O_{40}$ is a monolayer. TS measurements taken with the STM tip positioned atop the corrugations in Figure 4, irrespective of contrast, showed NDR behavior in the $I-V$ spectra. The frequency of observation of NDR in the $I-V$ spectra of the corrugations (normalized by the total number of TS measurements for comparative purposes) is plotted as a function of the applied potential at which it was observed, as shown in Figure 10. The observation of NDR features in the $I-V$ spectra is consistent with earlier STM studies[31,33−35] of HPA monolayers. The NDR peak voltage distributions in Figure 10 can be compared to the NDR peak distributions from $I-V$ spectra of pure $H_3PW_{12}O_{40}$ and $H_3PMo_{12}O_{40}$ monolayers represented in Figures 11 and 12, respectively.

In general, TS measurements taken on the "bright" corrugations showed NDR features at -1.15 ± 0.05 V, while those taken on the "dim" corrugations showed them at -0.90 ± 0.05 V. Figure 10 demonstrates that the distribution of NDR peak voltages observed for the mixture is bimodal, with statistical means of -1.15 ± 0.05 V and -0.90 ± 0.05 V. It is noteworthy here that the distribution of NDR peak voltages for $H_3PMo_{12}O_{40}$ in the mixture is slightly narrower than that for the pure components. The two lobes of the distribution in Figure 10 can be assigned to the two components. Those points with NDR voltages between -1.1 and -1.3 V can be assigned to $H_3PW_{12}O_{40}$ and those between -0.95 and -0.80 V can be assigned to $H_3PMo_{12}O_{40}$. Those at -1.0 and -1.05 V could, in principle, be either, but these uncertain points represent only about 10% of the total. The scatter in the data is not surprising at all, given the scatter in similar histograms (Figures 11 and 12) for NDR voltages of the pure components. The statistical means determined by fitting the data for the pure components to normal (Gaussian) curves were -1.14 ± 0.09 V for $H_3PW_{12}O_{40}$ and -0.95 ± 0.09 V for $H_3PMo_{12}O_{40}$. On the basis of the TS measurements, we conclude that the "bright" corrugations are observed when tunneling to the $[PW_{12}O_{40}]^{3-}$ anions and the "dim" corrugations are observed when tunneling to the $[PMo_{12}O_{40}]^{3-}$ anions. It is important to note that not all regions imaged showed such variations in contrast and $I-V$ spectra, suggesting that there may also have been regions on the surface that were predominantly occupied by one kind of HPA.

All of the $I-V$ data for each sample are averages of data collected using at least three different tips. Different sets of tips were used for the pure components and for the mixtures. Yet while such precautions are necessary in obtaining useful and reproducible $I-V$ data, they do not obviate the fact that the tip structure may change electronically during or between TS measurements, or that the tunneling area (~5 Å diameter) may vary significantly as the tip is moved supposedly from corrugation (anion) to corrugation (anion). Despite such uncertainties regarding tip characteristics, it is apparent from Figure 10 that the NDR voltages of the mixed array of $H_3PW_{12}O_{40}$ and $H_3PMo_{12}O_{40}$ can be represented as a combination of the NDR peak voltages of pure $H_3PW_{12}O_{40}$ and $H_3PMo_{12}O_{40}$.

Conclusions

STM studies of mixed arrays of Keggin-type HPAs deposited on graphite were carried out. The mixture of Keggin-type HPAs, $H_3PW_{12}O_{40}$ and $H_3PMo_{12}O_{40}$, with identical net anionic charges and identical charge-compensating cations (protons) formed well-ordered two-dimensional arrays similar to those formed by their pure components. The periodicities of the arrays were consistent with the shape and dimension of pure Keggin-type HPAs. STM images of the mixed arrays of $H_3PW_{12}O_{40}$ and $H_3PMo_{12}O_{40}$ (deposited from an equimolar mixed solution) showed that some corrugations were brighter than others; the ratio of bright to dim corrugations was almost unity and their distribution within the ordered array on the surface appeared to be fairly random. TS measurements demonstrated that the bright corrugations were $[PW_{12}O_{40}]^{3-}$ anions and that the less bright ones were $[PMo_{12}O_{40}]^{3-}$ anions. Thus HPAs with identical geometric structures and sizes can be distinguished based on differences in their electronic properties using STM operated in air, as the contrast in the STM image is related to the LDOS of the sample.

Acknowledgment. I.K.S. acknowledges fellowship support from the Seoam Scholarship Foundation. The Topometrix TMX-2010 was acquired via an equipment grant from the U.S. Department of Energy.

References and Notes

(1) Karanamuni, J.; Kurtz, R. L.; Stockerbauer, R. L. *Surf. Sci*. **1999**, *442*, 223.
(2) Wan, L.-J.; Shundo, S.; Inukai, J.; Itaya, K. *Langmuir* **2000**, *16*, 2164.
(3) Chen, Q.; Perry, C. C.; Frederick, B. G.; Murry, P. W.; Haq, S.; Richardson, N. V. *Surf. Sci*. **2000**, *446*, 63.
(4) Upward, M. D.; Beton, P. H.; Moriarty, P. *Surf. Sci*. **1999**, *441*, 21.
(5) Sato, T.; Kitamura, S.-I.; Iwatsuki, M. *Surf. Sci*. **2000**, *445*, 130.
(6) Krenn, G.; Eibl, C.; Mauritsch, W.; Hebenstreit, E. L. D.; Varga, P.; Winkler, A. *Surf. Sci*. **2000**, *445*, 343.
(7) Noh, J.; Hara, M. *Langmuir* **2000**, *16*, 2045.
(8) Chiang, S.; Wilson, R. J.; Mate, C. M.; Ohtani, R. *J. Microsc.* **1988**, *152*, 567.
(9) Hallmark, V. M.; Chiang, S.; Brown, J. K.; Wöll, Ch. In *Synthetic Microstructures in Biological Research*; Schnur, J. M., Peckerar, M., Eds.; Plenum Press: New York, 1992; p 79.
(10) Boland, J. J.; Villarrubia, J. S. *Science* **1990**, *248*, 838.
(11) Wouda, P. T.; Nieuwenhuys, B. E.; Schmid, M.; Varge, P. *Surf. Sci*. **1996**, *359*, 17.
(12) Hipps, K. W.; Lu, X.; Wang, X. D.; Mazur, U. *J. Phys. Chem*. **1996**, *100*, 11207.
(13) Lu, X.; Hipps, K. W.; Wang, X. D.; Mazur, U. *J. Am. Chem. Soc*. **1996**, *118*, 7197.
(14) Cernota, P. D.; Yoon, H. A.; Salmeron, M.; Somorjai, G. A. *Surf. Sci*. **1998**, *415*, 351.
(15) Silva, S. L.; Patal, A. A.; Pham, T. M.; Leibsle, F. M. *Surf. Sci*. **1999**, *441*, 351.
(16) Gimzewski, J. K.; Stoll, E.; Schlittler, R. R. *Surf. Sci.* **1987**, *181*, 267.
(17) Boland, J. J.; Villarrubia, J. S. *Phys. Rev. B* **1990**, *41*, 9865.
(18) Piancastelli, M. N.; Motta, N.; Sgarlata, A.; Balzarotti, A.; De Crescenzi, M. *Phys. Rev. B* **1993**, *48*, 17892.
(19) Hamers, R. J.; Wang, Y. *Chem. Rev.* **1996**, *96*, 1261.
(20) Hersam, M. C.; Guisinger, N. P.; Lyding, J. W. *J. Vac. Sci. Technol. A* **2000**, *18*, 1349.
(21) Johansson, M. K.-J.; Gray, S. M.; Johansson, L. S. O. *J. Vac. Sci. Technol., B* **1996**, *14*, 1015.
(22) Bode, M.; Pascal, R.; Wiesendanger, R. *J. Vac. Sci. Technol., A* **1997**, *15* (3), 1285.
(23) Keggin, J. F. *Nature* **1933**, *131*, 908.
(24) Brown, G. M.; Noe-Spirlet, M.-R.; Busing, W. R.; Levy, H. A. *Acta Crystallogr., Sect. B* **1977**, *B33*, 1038.
(25) Kozhevnikov, I. V. *Catal. Rev.—Sci. Eng*. **1995**, *37*, 311.
(26) Kaba, M. S.; Barteau, M. A.; Lee, W. Y.; Song, I. K. *Appl. Catal. A* **2000**, *194*, 129.
(27) Okuhara, T.; Mizuno, N.; Misono, M. *Adv. Catal*. **1996**, *41*, 113.
(28) Song, I. K.; Kaba, M. S.; Barteau, M. A.; Lee, W. Y. *Catal. Today* **1998**, *44*, 285.
(29) Keita, B.; Nadjo, L. *J. Electroanal. Chem*. **1990**, *287*, 149.
(30) Song, I. K.; Kaba, M. S.; Coulston, G.; Kourtakis, K.; Barteau, M. A. *Chem. Mater*. **1996**, *8*, 2352.
(31) Kaba, M. S.; Song, I. K.; Barteau, M. A. *J. Phys. Chem.* **1996**, *100*, 19577.
(32) Song, I. K.; Kaba, M. S.; Barteau, M. A. *J. Phys. Chem*. **1996**, *100*, 17528.
(33) Kaba, M. S.; Song, I. K.; Barteau, M. A. *J. Vac. Sci. Technol., A* **1997**, *15* (3), 1299.
(34) Kaba, M. S.; Song, I. K.; Duncan, D. C.; Hill, C. L.; Barteau, M. A. *Inorg. Chem.* **1998**, *37*, 398.
(35) Kinne, M.; Barteau, M. A. *Surf. Sci*. **2000**, *447*, 105.
(36) Eigler, D. M.; Schweizer, E. K. *Nature* **1990**, *344*, 524.
(37) Tersoff, J. In *Scanning Tunneling Microscopy and Spectroscopy, Theory, Techniques and Applications*; Bonnell, D. A., Ed.; VCH Publishers: New York, 1993.
(38) Binnig, G.; Quate, C.; Gerber, Ch. *Phys. Rev. Lett.* **1986**, *56*, 930.
(39) Winterlin, J.; Behm, R. J. In *Scanning Tunneling Microscopy I*; Güntherodt, H.-J., Wiesendanger, R., Eds.; Springer-Verlag: New York, 1992; p 42.
(40) Magonov, S. N.; Whangbo, M.-H. *Adv. Mater*. **1994**, *6*, 355.
(41) Whangbo, M.-H.; Hoffman, R. *J. Am. Chem. Soc.* **1978**, *100*, 6093.
(42) Magonov, S. N.; Whangbo, M.-H. *Surface Analysis with STM and AFM, Experimental and Theoretical Aspects of Image Analysis*; VCH Publishers: New York, 1996; p 3.
(43) Weber, R. S. *J. Phys. Chem*. **1994**, *98*, 2999.
(44) Chen, G.; Goddard, W. A., III. *Phys. Rev. B* **1994**, *50*, 8035.
(45) Müssig, H.-J.; Krüger, D.; Hinrich, S.; Hansson, P. O. *Surf. Sci*. **1994**, *314*, L884.
(46) Petukhov, A. G.; Demchenko, D. O.; Chantis, A. N. *J. Vac. Sci. Technol., B* **2000**, *18*, 2109.